Research Article | Vol. 28, No. 14 / 6 July 2020 / Optics Express 20473
Optics EXPRESS

High-energy soliton fission dynamics in multimode GRIN fiber

MARIO ZITELLI,[1,*] FABIO MANGINI,[2] MARIO FERRARO,[1] ALIOUNE NIANG,[2] DENIS KHARENKO,[3,4] AND STEFAN WABNITZ[1,3]

[1]Department of Information Engineering, Electronics and Telecommunications (DIET), Sapienza University of Rome, Via Eudossiana 18, 00184 Rome, Italy
[2]Department of Information Engineering (DII), University of Brescia, Via Branze 38, 25123 Brescia, Italy
[3]Novosibirsk State University, Pirogova 1, Novosibirsk 630090, Russia
[4]Institute of Automation and Electrometry SB RAS, 1 ac. Koptyug ave., Novosibirsk 630090, Russia
[*]mario.zitelli@uniroma1.it

Abstract: The process of high-energy soliton fission is experimentally and numerically investigated in a graded-index multimode fiber. Fission dynamics is analyzed by comparing experimental observations and simulations. A novel nonlinear propagation regime is observed, where solitons produced by the fission have a nearly constant Raman wavelength shift and same pulse width over a wide range of soliton energies.

1. Introduction

The concept of optical soliton propagation in multimode (MM) fibers was introduced in the literature nearly forty years ago [1–3]. From a fundamental point of view, multimode fiber solitons provide an experimentally easily accessible example of spatiotemporal solitons or light bullets, where dispersion and diffraction are balanced by nonlinearity at the same time [4]. It is particularly interesting to explore the dynamics of these fascinating and elusive nonlinear wave packets, as the power of the pulse approaches the critical value for self-focusing. In bulk Kerr media, self-similar optical wave collapse occurs whenever self-focusing due to the Kerr effect overcomes diffraction [5]. On the other hand, in a MM fiber the linear index profile of the fiber acts as a guiding potential for light, which may end up with a stabilizing action for spatiotemporal solitons. Analytical approximate solutions using the variational approach predict the formation of stable spatiotemporal solitons in the anomalous dispersion regime with a positive nonlinearity [6,7]. To date, the dynamics of spatiotemporal solitons at powers approaching the multi-dimensional collapse power remain largely unexplored in fiber optics experiments. A main objective of this work is to bridge this gap of knowledge.

Although MM soliton generation in a graded-index (GRIN) fiber was first experimentally demonstrated back at the end of the 80's [8], it is not until recent years that nonlinear optics in MMFs fibers has seen a revival of interest [9,10]. In 2013, Renninger and Wise observed that MM solitons result from the simultaneous compensation of chromatic dispersion and modal dispersion via the Kerr nonlinearity of the MM fiber [11]. The associated Raman-induced MM soliton self-frequency shift (SSFS) in GRIN MM fibers was investigated in a low pulse energy (up to 3 nJ) situation, where the MM soliton was essentially carried by the fundamental mode of the MM fiber. The spatiotemporal behavior of MM solitons, including their formation and fission, was later investigated by Wright et al. with input beams leading to input energy distribution among several guided modes [12]; Raman MM solitons at 2100 nm could be generated from a GRIN fiber, by using 500 fs input pulses at 1550 nm, with energies up to 30 nJ.

In the regime of highly nonlinear ultrashort pulse propagation in the anomalous-dispersion regime of a GRIN MM fiber, a variety of spatio-temporal effects was observed [13]. By adjusting the spatial initial conditions, megawatt, ultra-short pulses, tunable between 1550 and 2200 nm,

#394896 https://doi.org/10.1364/OE.394896
Journal © 2020 Received 17 Apr 2020; revised 8 Jun 2020; accepted 8 Jun 2020; published 25 Jun 2020

Optics EXPRESS

could be generated from the 1550 nm pump wavelength [13,14]. When propagating in a few-mode GRIN MM fiber, it was shown that MM solitons display a continuous range of spatiotemporal properties, that depend on their modal composition [15]. The generation of 120 fs MM solitons was reported, with higher energies with respect to single mode (SM) solitons, a property attributed to the transverse spatial degrees of freedom that result from the fiber supporting multiple spatial eigenmodes. The modal distribution of the input beam plays an important role in controlling the different frequency conversion processes that shape the output spectrum [16]. Specifically, the interplay of soliton fission processes, stimulated Raman scattering, dispersive wave generation and intermode four-wave mixing. Whereas in the case of step-index fibers, the presence of Raman scattering may lead to novel soliton self-mode conversion effects [17].

The impact of self-imaging on soliton propagation in GRIN MM fibers was recently investigated using a simplified model [18], based on the SM generalized nonlinear Schrödinger equation (GNLSE) with a spatially varying effective mode area [19], evolving according to the variational approach (VA) [20]. The Raman-induced fission of higher-order solitons into fundamental solitons was numerically described in terms of the SM model [21]. The experimental validation of the SM soliton fission theory and the subsequent SSFS of different Raman solitons in MM GRIN fibers has not yet been reported.

In this paper, we experimentally study spatiotemporal soliton generation and propagation in a MM fiber, for input femtosecond pulses in the anomalous dispersion regime, with up to several MWs of peak power, approaching the 8 MW critical value for spatiotemporal pulse collapse [22].

Specifically, we analyze the fission in a GRIN fiber of high input energy (up to 550 nJ, which is the upper limit set by the irreversible damage of the fiber), high-order MM solitons with about 100 femtosecond temporal duration. The input multi-soliton pulses undergo Raman-induced fission into several individual MM solitons.

In Section 3.3 we experimentally observe, and numerically confirm in Section 3.2, that MM solitons spontaneously self-organize into a wavelength multiplex, intended as a multitude of well separated spectral lobes, before undergoing SSFS. Moreover, in Section 3.5 we determine the temporal duration of the different generated Raman solitons as a function of their energy, and discover that, for soliton energies above 15 nJ, their temporal duration remains nearly a constant. Whereas their peak power varies, so that at each wavelength the Kerr nonlinearity exactly balances the local value of chromatic dispersion, as required by the fundamental soliton condition. This means that, at relatively high energies, the fission of the input higher-order soliton leads to an optimal funneling of the input energy into fundamental solitons, which minimizes the amount of dispersive waves or radiation, as analytically shown by Kodama et al. [23]. To our knowledge, this result has not been previously reported, even in the well-studied case of SM solitons. In Section 3.7 and 3.6 we estimate the order of the generated solitons, and their output transverse intensity distribution, respectively, showing that they are indeed fundamental spatiotemporal solitons with a bell-shaped beam profile. It has been pointed out that the description of the dynamics of solitons in GRIN fibers may be reduced to that of SM solitons [18,19,21]. Indeed, in Section 3.4 we experimentally confirm that the SSFS formula for SM solitons [24] accurately describes the red-shift of Raman solitons with energies up to 15 nJ.

Remarkably, in this work we unveil a new nonlinear propagation regime in MM fibers, for peak powers in the MW range, approaching the spatiotemporal collapse value. As discussed in Section 3.1, this regime is characterized by the presence of a strong nonlinear absorption, which clamps the transmitted energy at the fiber output. In sections 3.3 and 3.4 we show that, as a result of this nonlinear loss mechanism, which limits the available optical energy in the fiber, the SSFS of Raman solitons is suppressed. For input pulse energies above 100 nJ, a significant side-scattering of blue photo-luminescence, visible and near-infrared radiation is observed in the first few centimeters of fiber, as discussed in details elsewhere [10,22]. Blue light appears at the points of peak intensity, which are determined by the periodic spatial beam compression resulting

Optics EXPRESS

from self-imaging (SI) of the input multimode beam. The emission of photo-luminescence is due to multiphoton absorption by defects in the Germanium doped fused silica fiber [25].

2. Methods

2.1. Experimental setup

As shown in Fig. 1, the experimental setup used for the generation of high-energy MM solitons consists of an ultra-short laser system, involving a hybrid optical parametric amplifier (OPA) of white-light continuum (Lightconversion ORPHEUS-F), pumped by a femtosecond Yb-based laser (Lightconversion PHAROS-SP-HP), generating pulses at 25 to 100 kHz repetition rate, with Gaussian beam shape (M^2=1.3). The pulse shape was measured using an autocorrelator (APE PulseCheck type 2), resulting in a sech temporal shape, with a typical 130 fs pulse width. The laser beam was focused by a 30 mm lens into a 30 cm span of GRIN fiber, with an input diameter of approximately 20 μm at $1/e^2$ of peak intensity. The input pulse wavelength is set at 1550 nm, and its energy is varied between 0.1 and 550 nJ by means of a variable external attenuator.

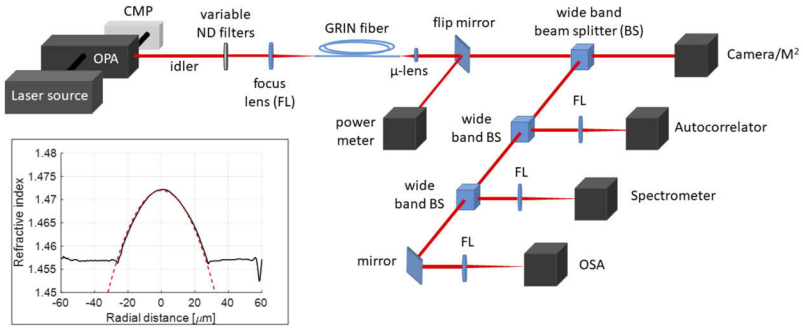

Fig. 1. Schematic of the experimental setup and measured index profile of the GRIN fiber (inset).

The fiber index profile had a core radius r_c=25 μm, cladding radius 62.5 μm, and a cladding index n_{clad}=1.457, with the relative core-cladding index difference Δ=0.0103. The fiber parameters were measured along with the index profile by a NR-9200 Optical Fiber Analyzer, as shown in the inset of Fig. 1. The index measurement was based on the refracted near field. After the cleave, the fiber was immersed in a calibrated oil solution, and illuminated with a single mode laser at 667 nm. A scanning of the fiber face allowed to obtain the refractive index profile, with a resolution of 0.4 μm. At the fiber output, a micro-lens followed by a second lens focused the beam into an optical spectrum analyzer (OSA) (Yokogawa AQ6370D) and a real-time multiple octave spectrum analyzer (Fastlite Mozza), with wavelength ranges of 600-1700 nm and 1000-5000 nm, respectively. A miniature fiber optics spectrometer (Ocean Optics USB2000+), with 200-1100 nm spectral range, was also used. The output radiation was passed through different long-pass or band-pass optical filters, in order to isolate the individual Raman solitons from the residual radiation. Output soliton spectra were analyzed by using a sech^2 fit of each corresponding lobe in the output spectrum. This permitted us to determine the soliton central wavelength and bandwidth. The MM soliton energy was extracted, and compared with the total spectral power as measured by a power meter. The output soliton pulse width was calculated by assuming a transform limited time-bandwidth product, and checked by the autocorrelator. The output near field was also projected on a near-infrared (NIR) camera (Gentec Beamage-4M-IR), in order to optimize input coupling, and measure the output transverse intensity distribution. The beam quality factor M^2 of the output beam was measured with a calibrated and automated optical

Optics EXPRESS

system (Gentec Beamage M2). Input and output average powers were measured by a thermopile power meter (GENTEC XLP12-3S-VP-INT-D0).

2.2. Numerical model

Our numerical model for simulating high-energy optical pulse propagation in a GRIN MM fiber is based on the $(3D+1)$ GNLSE (or Gross-Pitaevskii equation [26]) in its vectorial form, involving a single field for each polarization, including all frequencies and modes:

$$\begin{aligned}\frac{\partial A_p(x,y,z,t)}{\partial z} &= \frac{i}{2k}\left(\frac{\partial^2 A_p}{\partial x^2}+\frac{\partial^2 A_p}{\partial y^2}\right) - i\frac{\beta_2}{2}\frac{\partial^2 A_p}{\partial t^2} + \frac{\beta_3}{6}\frac{\partial^3 A_p}{\partial t^3} + i\frac{\beta_4}{24}\frac{\partial^4 A_p}{\partial t^4} - \frac{\alpha}{2}A_p + \\ &+ i\frac{k}{2}\left[\frac{n^2(x,y)}{n_0^2}-1\right]A_p + i\gamma\left(1+iK_2+\frac{i}{\omega_0}\frac{\partial}{\partial t}\right)\left[(1-f_R)A_p\left(|A_p|^2+\frac{2}{3}|A_q|^2+\frac{1}{3}A_p^2 e^{-2i\omega_0 t}\right)+\right. \\ &\left. + f_R A_p\int_{-\infty}^{t} d\tau h_R(\tau)\left(|A_p(t-\tau)|^2+\frac{2}{3}|A_q(t-\tau)|^2\right)\right],\end{aligned} \quad (1)$$

with $\gamma = n_2\frac{2\pi}{\lambda}$, $k = 2\pi n_0/\lambda$, $K_2 = \frac{\alpha_2}{2\gamma}$, and $f_R = 0.18$. In Eqs. (1), the two polarizations $p, q = x, y$ are nonlinearly coupled. Terms in the right-hand side of Eq. (1) account for: transverse diffraction, second, third and fourth-order dispersion, linear loss, the waveguiding term with refractive index profile $n(x, y)$ and effective core index n_0, Kerr and Raman nonlinearities (with nonlinear coefficient γ and fraction f_R, respectively). In Eqs. (1) we neglect the contribution of polarization mode dispersion: we numerically verified that its effects are negligible for the short fiber lengths (up to 30 centimeters) involved in our experiments. Nonlinearities include self-steepening, third-harmonic generation (THG) and two-photon absorption (TPA) (with coefficient α_2). The model of Eq. (1) is alternative to that based on coupled equations for the fiber modes [27], which requires a preliminary knowledge of the power distribution among the fiber modes at the fiber input. Random phase noise was added to the input field, in order to describe the generation of intensity speckles and to seed dispersive waves, which are typically observed in multimode fibers. Random changes in the fiber core diameter have also been introduced, although they produced negligible effects over the considered fiber lengths.

In simulations, we used the following GRIN fiber parameters: core radius, cladding radius, and relative index difference are already provided in the experimental setup subsection; dispersion parameters are $\beta_2 = -22\,\mathrm{ps}^2/\mathrm{km}$ at 1550 nm, $\beta_3 = 0.132\,\mathrm{ps}^3/\mathrm{km}$, $\beta_4 = -5\times10^{-4}\,\mathrm{ps}^4/\mathrm{km}$; nonlinear parameters are $n_2 = 2.7\times10^{-20}\,\mathrm{m}^2/\mathrm{W}$, $\alpha_2 = 1\times10^{-16}\,\mathrm{m/W}$ (this value was justified by a best fit of the SSFS observed in the experiments); $h_R(\tau)$ with the typical response times of 12.2 and 32 fs, respectively [28,29].

We included the wavelength dependence of the linear loss coefficient α, as reported for standard SM glass fibers [30]. For a 30 cm fiber length, linear losses considerably affect transmission at wavelengths above 2500 nm only, and are negligible for wavelengths considered in this work. In fact, we measured the relative energy transmission from the GRIN fiber, normalized to its value at 1550 nm, by using relatively low-power pulses (i.e., in linear propagation conditions) from our OPA, with a wavelength ranging from 1400 to 2500 nm. We determined that linear losses in the mid-infrared lead to less than 10% transmission drop up to 2300 nm (and reach a 50% drop only above 2500 nm). The input beam is modeled as a Gaussian beam with $w_0 = 10$ μm waist (20 μm diameter); we used a sech temporal shape with full-width-at-half-maximum (FWHM) pulse width $T_{\mathrm{FWHM}} = 130$ fs. The associated chromatic dispersion length is $L_d = T_0^2/|\beta_2| = 25$ cm, where $T_0 = T_{\mathrm{FWHM}}/1.763$.

Random phase noise was added at input for both polarizations. Two polarizations are launched at the fiber input with a variable spit ratio between 0.5 and 1, the last value corresponding to a single polarization. Although the model of Eqs. (1) considers all modes merged in a single field, our fiber launch conditions produce, in the linear regime, three axial-symmetric modes with

Optics EXPRESS

power fraction: 0.84, 0.13, 0.02, respectively; higher-order modes can be neglected. In order to check the effective generation of multimodal solitons, simulations were also performed by using the coupled mode equations model from Refs. [27,31]. In the next Section 3., we shall compare numerical simulations using Eqs. (1) to experimental results. Moreover, we confirm the modal decomposition of Raman multimode solitons generated by the input multi-soliton fission by using the model from Ref. [27], as implemented by a modified version of the open source parallel numerical solver of Wright et al. [31].

3. Results and discussion

Here we report our experimental studies of MM soliton fission dynamics, using the setup of Subsection 2.1. We considered relatively short GRIN fiber spans of length up to 30 cm. For a better understanding of the complex MM nonlinear effects involved, we compared observations with numerical simulations with the full MM model described in Subsection 2.2, as well as with the analytical theory for SM Raman solitons [24]. All figure captions specify if the curves refer to either experimental or simulation data.

3.1. Nonlinear loss

We observed a strong output energy clamping for an input pulse energy E_{in}>100 nJ. Figure 2(a) shows the measured output energy vs. input energy, in the overall detected spectral bandwidth (red curve with stars), or after insertion of a filter that strongly attenuates all wavelengths below 1100 nm (black curve with diamonds). In both cases, energy losses are limited from zero to below 20% for input energies E_{in} up to 100 nJ. For E_{in} > 150 nJ, the output energy saturates to a nearly constant value. This output energy clamping is not affected by changing the laser pulse repetition rate, while maintaining the input pulse energy unchanged, indicating that thermal effects are not involved in the output energy loss.

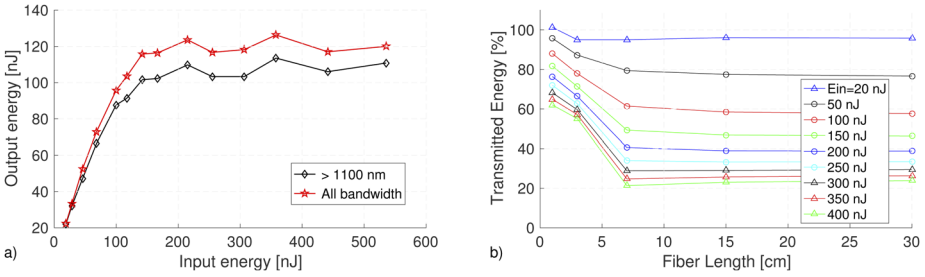

Fig. 2. a) Experimental output pulse energy vs. input pulse energy, in the overall bandwidth or for wavelengths above 1100 nm. b) Fraction of transmitted energy vs. fiber length for different input pulse energies.

Figure 2(b) is the result of a cutback experiment (performed with a 50 mm input lens), illustrating the dependence of nonlinear energy loss upon fiber length (starting from 1 cm), for several values of the input pulse energy. Here the loss is determined in terms of the transmitted energy by the fiber or the ratio of output to input pulse energy. This ratio is normalized to the fiber coupling efficiency at low powers (equal to 45%), so that the transmitted energy at low powers is 100% for all fiber lengths. Figure 2(b) shows that losses mainly occur over the first 7 cm of fiber (and particularly over the first cm already), and remain negligible in the remaining fiber section. The strong drop of transmitted energy as the input pulse energy grows larger confirms the nonlinear nature of the loss mechanism. We ascribe the nonlinear loss to multi-photon absorption by defects of the Germanium doped fiber [25], leading to the side-emission of broadband blue photo-luminescence [10,22], as well as to scattering from the cladding of NIR radiation, THG,

Optics EXPRESS

and visible dispersive wave sidebands [13,14]. Nonlinear loss is most efficient at the points of peak beam intensity, generated by SI [20] over the first few cm of fiber. A maximum intensity is reached during the input MM soliton pulse fission phase, occurring in the first centimeters of fiber, were the peak power reaches several MWs [10,19]. We defer a detailed comparison between experiments and theory of multi-photon absorption and side-scattering induced nonlinear loss processes in the GRIN fiber to a subsequent publication.

Summarizing, two energy regimes are observed in Fig. 2(a) and 2(b). In the first regime, for $E_{\rm in}$<100 nJ, nonlinear losses are negligible. Whereas for 100<$E_{\rm in}$<550 nJ, significant nonlinear loss occurs over the first few cm of fiber, and the output energy is clamped. In the following, we will refer to the first and second regime as "linear-loss" and "nonlinear-loss" regimes, respectively. We also observed that, for input energies above 550 nJ (i.e., about 2.1 MW input peak power), the beam undergoes catastrophic collapse with permanent damages at the input and across the fiber length.

3.2. Fission dynamics

In order to analyze the MM soliton fission process and compare it with existing SM soliton theory predictions, we carried out a series of simulations in the "linear-loss" regime, where the impact of TPA and higher-order multi-photon absorption can be neglected.

Figure 3(a) shows the evolution of the intensity spectrum as a function of fiber length, for the input energy of 90 nJ. As can be seen, the fission of the input pulse leads to a complex wavelength multiplex of MM solitons, which is generated at the short distance of about ten centimeters. The corresponding wavelength shifts of solitons generated by the fission are nonadiabatic, i.e., they occur over a much shorter distance than the length required to obtain an equivalent wavelength shift via the SSFS formula from SM soliton perturbation theory [24,32]

$$\Delta\lambda_j(z) = \lambda_{\rm f,j} + \frac{4\lambda_{\rm f,j} n_2 T_R E_{\rm s,j}}{15c\pi w_j^2 T_0 j^3}\left(z - z_f\right), \tag{2}$$

where T_R=3 fs is the Raman response time, z is the fiber propagation coordinate, $T_0 j$=T_j/1.763 with T_j the soliton FWHM pulse width, $\lambda_{\rm f,j}$ is the wavelength of the j-th soliton generated by the fission, $w_{\rm j}$ is its effective bullet waist, and $E_{\rm s,j}$ is its energy. Now, for a fundamental SM soliton, the energy reads as

$$E_{\rm s,j} = \frac{\lambda|\beta_2|w_j^2}{n_2 T_0 j}. \tag{3}$$

Note that, in applying the SSFS formula Eq. (2), the distance z is measured starting from the point of soliton fission, say, z_f. In other words, after the fission process, each resulting MM soliton in the wavelength multiplex undergoes a slow adiabatic frequency shift, which may be described according to the second term in the right-hand side of Eq. (2).

In GRIN fibers, the soliton waist is a periodic function of distance with the SI period $z_{\rm SI} = \pi r_{\rm c}/\sqrt{2\Delta}$= 0.55 mm (see Fig. 3(d)) [19,20]. Since $z_{SI} \ll L_d$, it has been proposed that, for describing GRIN soliton propagation, one may consider an effective beam waist, which results from computing the path-average value of the nonlinear coefficient of the fiber $\hat{\gamma}(z) = \gamma/(\pi w_j^2(z))$ [18]. That is, one may set $w_j^2 \simeq \sqrt{C} w_0^2$ in Eq. (2), where $C = A_{min}/A_{max} = w_{j,min}^2/w_{j,max}^2$ is the ratio of minimum to maximum effective area (waist square) of the bullets, and w_0 is the input beam waist.

When displaying the pulse power in the time domain, i.e., by integrating the field intensity across the transverse x, y axes, the simulation of Fig. 3(b) shows that the input pulse undergoes a temporal compression over the first 5 mm of fiber. Correspondingly, it reaches local peak powers up to several MWs until it experiences a soliton fission, thus producing a number of solitons, each with a comparable pulse width between 45 fs and 60 fs, and different peak powers, ranging

Optics EXPRESS

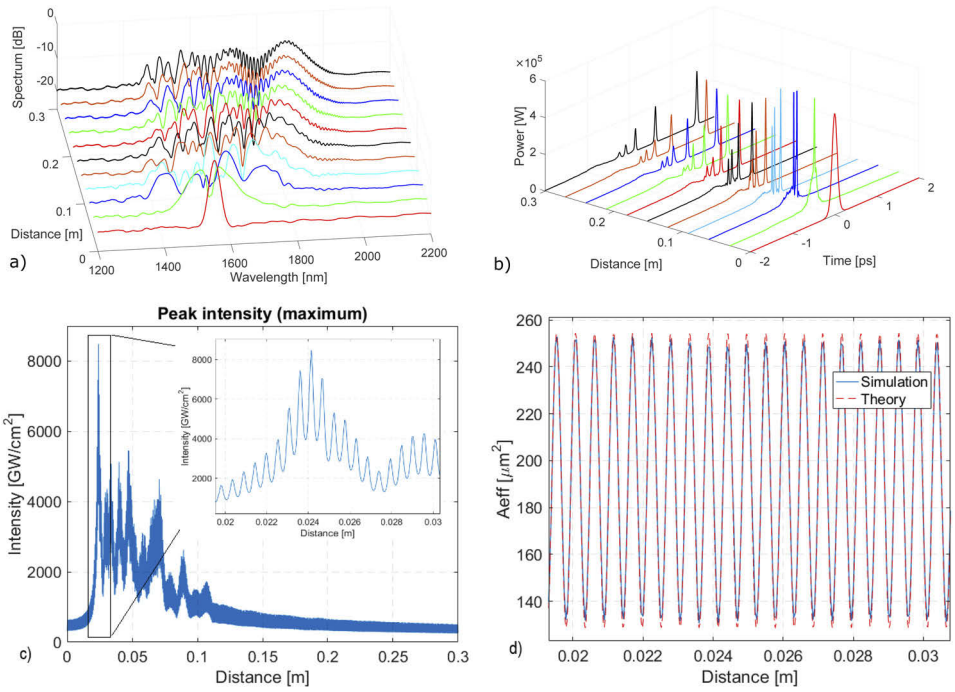

Fig. 3. Simulation of the a) spectra, and b) pulse power evolution with distance; case of 90 nJ input pulse energy; c) simulation of evolution of the peak intensity of the total field along the GRIN MMF; d) simulation of the evolution along the fiber of the effective area of the beam (blue curve), compared with the prediction of the variational theory (red dashed curve).

from few tens of kW up to 300 kW. The number M of generated solitons may arrive up to 5 when the input energy grows larger. In the "linear-loss"regime, the numerically generated solitons have energies below 20 nJ (peak powers below 300 kW). Figure 3(b) also shows the generation of dispersive waves with a negative delay, corresponding to anti-Stokes radiation. Our simulations show that those waves partially propagate in the cladding.

Figure 3(c) illustrates the evolution of the overall peak intensity vs. distance, for an input pulse energy of 90 nJ. As it can be seen, the field intensity undergoes an initial giant peak at around 2.5 cm of distance, followed by damped peaks up to the distance of 10 cm, where the fission process is complete.

In the spatiotemporal domain, the train of solitons generated after the fission of the input pulse corresponds to as many bullets. Soliton bullets experience a synchronous periodic SI in the transverse plane, with a period that corresponds remarkably well to the theoretical value, namely z_{SI}. All soliton bullets, after integration in time, possess similar minimum and maximum effective areas, in spite of their different wavelengths. The ratio of minimum to maximum effective area for all bullets is $C = 0.53$, in good quantitative agreement with the prediction of the VA [18–20], as it is shown in Fig. 3.(d) and in the inset of Fig. 3(c). From Fig. 3(d) we note that the periodicity of the effective area is not affected by the fission process.

The multimodal nature of the generated Raman solitons was confirmed by numerical simulations performed using a coupled mode equations model [27,31]. Figure 4(a) shows the output power of the individual modes composing the field, ranging from LP_{01} to LP_{03}. The model does not include any losses, and the input pulse asenergy is 100 nJ in this example. The five solitons are clearly multimodal, and conserve similar pulse widths between 39 and 47 fs. The temporal

Optics EXPRESS

walk-off due to group velocity mismatch between the fundamental and the LP_{02} or LP_{03} modes is equal to 0.256 ps/m and 0.520 ps/m, respectively. Therefore, in the absence of nonlinearity, pulse components in the first two modes would separate in time by 77 fs. On the other hand, Fig. 4(a) shows that all three modes remain superimposed in time, owing to the nonlinear compensation of modal dispersion. In Fig. 4(b) we show the corresponding output spectrum, with a Raman wavelength shift up to 2050 nm.

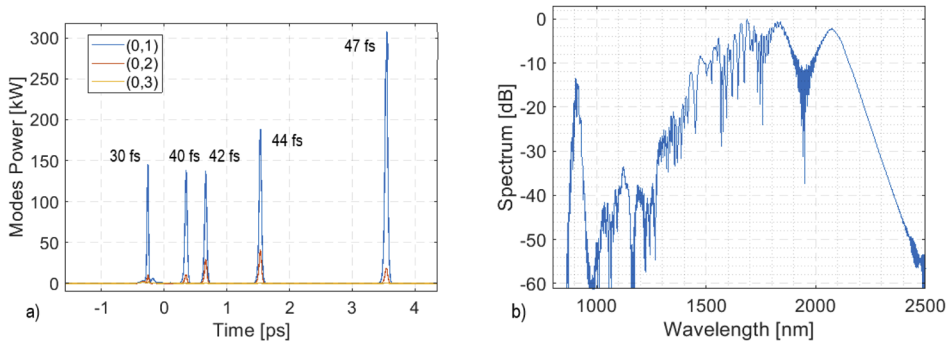

Fig. 4. Coupled mode simulation result showing the generation of five Raman solitons at the output of a 30 cm long GRIN fiber: (a) output power in the first three radially symmetric modes; (b) corresponding spectral intensity.

3.3. *Soliton spectra*

In this Subsection, we compare the predictions of Subsection 3.2 to the experiments. Moreover, we experimentally investigate the transition from the "linear-loss" to the "nonlinear-loss" propagation regime, and its impact on MM soliton fission, followed by the SSFS of fundamental MM solitons.

To disclose the details of high-order MM soliton fission, and the subsequent SSFS dynamics, we carried out a cutback experiment. Figure 5 illustrates the length dependence of the output spectrum, for E_{in}=300 nJ. A wavelength multiplex of fundamental Raman MM solitons appears at 7 cm, as the outcome of high-order MM soliton fission. In the first 3 cm of fiber, no Raman MM solitons are visible, since the fission process has not yet been completed. The generation

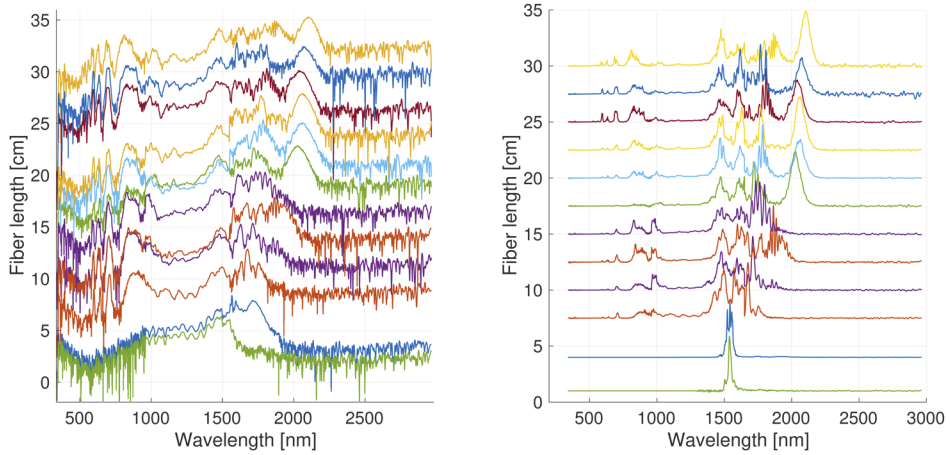

Fig. 5. Cutback experiment at 300 nJ input energy. Experimental output intensity spectra in log scale (left) and in linear scale (right)

Optics EXPRESS

of anti-Stokes dispersive wave sideband series (originating from spatiotemporal MM soliton oscillations [13,14]) is visible for wavelengths below 900 nm. A close inspection of the spectra shows that visible sidebands experience a progressive, weak blue-shift as the distance grows larger.

Figure 6, showing the experimental output spectra in a linear scale (with a GRIN fiber length of 30 cm) for several values of the input energy, illustrates well the transition from the "linear-loss" to the "nonlinear-loss" regimes. As can be seen, a progressively larger number of MM Raman solitons is generated as E_{in} grows larger. Individual MM solitons undergo different amounts of SSFS.

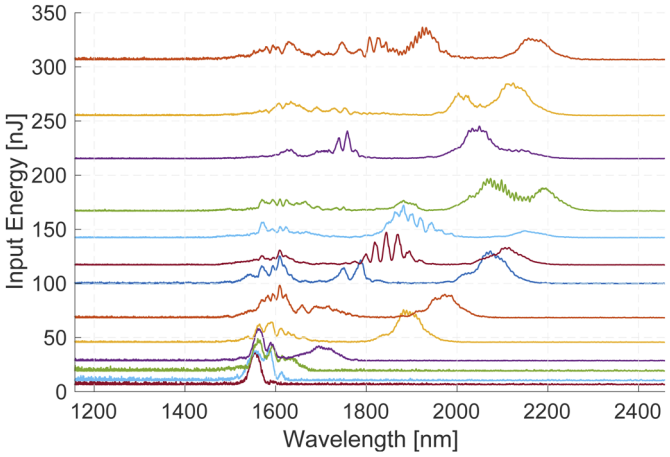

Fig. 6. Experimental output spectra in linear scale, from a GRIN fiber of 30 cm length, for several values of the input energy. Points where spectra cross the vertical axis indicate the corresponding input pulse energy.

In the "nonlinear-loss" propagation regime, i.e., for E_{in}>150 nJ, the Raman-induced wavelength shift halts when the soliton wavelength approaches 2200 nm. This occurs because the output energy remains clamped at 120 nJ for all input energies above 150 nJ (see Fig. 2(a)). We would like to underline that the observed output energy clamping cannot be ascribed to the linear multiphonon absorption of silica in the mid-infrared. As a matter of fact, Figs. 5 and 6 show that the wavelengths of Raman solitons always remain below 2200 nm: up to this wavelength, we measured a linear transmission loss of less than 10%. In addition, Fig. 5, for 300 nJ of input energy, shows that over the first 10 cm of fiber, where more than 70% transmission loss occurs (see Fig. 2(b)), the spectrum only extends over the low-loss region below 2000 nm. Therefore, we conclude that the SSFS suppression must be due to the multiphoton absorption mechanism discussed in Subsection 3.1.

3.4. Soliton wavelengths

We extracted in Fig. 7 the measured wavelength of individual MM solitons that are generated by the higher-order soliton fission process. In Fig. 7, we display the soliton wavelength as a function of the total output energy above 1100 nm (measured after inserting a long-pass filter, in order to eliminate most of the generated THG and supercontinuum, while including all solitons). Data in Fig. 7 include MM solitons generated in both the "linear-loss" and in the "nonlinear-loss" regimes.

In Fig. 7, we refer to Raman 1, Raman 2 and Raman 3, as the solitons that experience the highest to the lowest Raman shift, respectively. Additional solitons, if present, are not displayed here. The experimental data, illustrated as dots, are provided where the output spectra provide

Optics EXPRESS

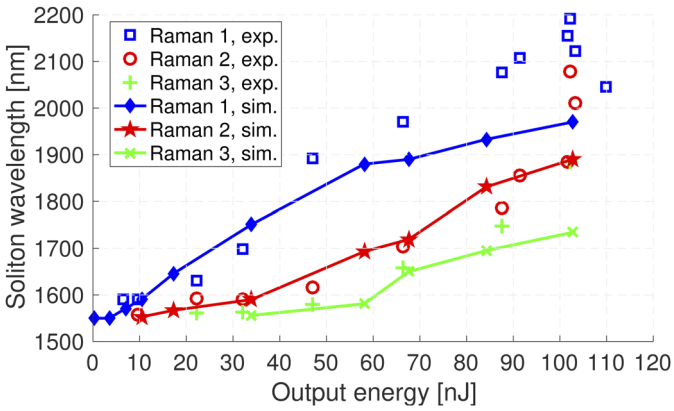

Fig. 7. Experimental wavelength shifts (empty squares, empty circles and crosses for solitons Raman 1, 2 and 3, respectively) vs. total output energy, after long-pass optical filtering at 1100 nm, at 30 cm of GRIN fiber. The wavelengths of the three Raman output solitons are ranged according to their absolute wavelength shift. Corresponding simulation results are indicated by solid lines with diamonds, stars and x-shaped crosses, respectively.

lobes that are easily fittable by using a sech^2 shape; other spectra have been discarded. Solid curves are the corresponding data from numerical simulations. In Fig. 7, numerical curves stop right above 100 nJ of output energy. As a matter of fact, simulations diverge for output energies above 110 nJ; numerics blow up due to beam filamentation after a few centimeters of fiber. As discussed in Subsection 3.1, in experiments the fiber damage threshold only occurs for relatively high input energies, above 550 nJ. We ascribe the discrepancy between simulations and experiments in the threshold for catastrophic self-focusing to the presence of a significant additional loss mechanism via multiphoton absorption and the associated side-scattering of photo-luminescence, a mechanism which is not included in our model.

Experimental data for the Raman 1, Raman 2, and Raman 3 solitons show that, for output energies up to 90 nJ ("linear-loss" regime), their wavelengths increase with output energy: the most shifted Raman 1 soliton reaches 2100 nm. For input energies above 90 nJ, high nonlinear losses provide a nearly constant output energy: as a result, an irregular distribution of soliton wavelengths appears in Fig. 7, and the output energy is clamped to values below 110 nJ.

The difference between the "linear-loss" and the "nonlinear-loss" regimes is also clearly revealed by Fig. 8, providing experimental data (empty squares and empty circles) and numerical simulations (solid curves) of the wavelength of solitons Raman 1 and Raman 2, respectively, as a function of their output energy, E_s. For experimental data, the soliton energy was directly measured as described in Section 3.5. Here the black dashed line is analytically obtained from the SM SSFS equation 2, where we used an effective bullet waist equal to its path-average value, $w_j^2 \simeq \sqrt{C} w_0^2$, which leads to SSFS enhancement. Moreover, we inserted the pulse width and wavelength λ of the corresponding output soliton from simulations; the dispersion β_2 is calculated at the wavelength of each soliton. Figure 8 shows that, in the "linear-loss" regime, and up to E_s=15 nJ, the wavelength of both Raman solitons increases with soliton energy, in excellent agreement with the SSFS formula Eq. (2), and with numerical simulations.

On the other hand, in the "nonlinear-loss" regime, which means here for Raman soliton energies $E_s > 15$ nJ, experimental data show that the soliton wavelengths remain approximately constant as the soliton energy grows larger up to 50 nJ. The soliton wavelenghts remain around 2100 nm for the Raman 1 soliton, and 1900 nm for the Raman 2 soliton, respectively. The results of Fig. 8 show that the dynamics of Raman solitons is dramatically affected by the presence of nonlinear loss, which clamps the total energy in the fiber to approximately 120 nJ (see Fig. 2(a)).

Optics EXPRESS

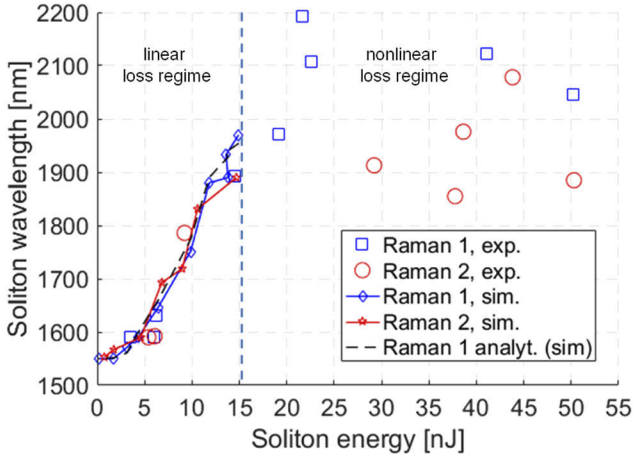

Fig. 8. Experimental data (empty squares and empty circles for solitons Raman 1 and 2, respectively) and numerical simulations (solid curves) of the wavelength of solitons Raman 1 and Raman 2 vs. soliton energy; black dashed line is obtained from Eq. (2).

Remarkably, Fig. 8 shows that almost all of the energy carried by the MM GRIN fiber can be captured by the two most red-shifted Raman solitons, whose total energy reaches up to 100 nJ.

3.5. Soliton durations

In this Section, we demonstrate that the numerical prediction as in Section 3.2 of the generation of a soliton wavelength multiplex with similar pulse widths is confirmed by our experimental analysis of the temporal duration of the different Raman solitons, which are generated by the fission process. Figure 9 compares experimental data and numerical simulations for the FWHM pulse width of different output MM Raman solitons, as a function of their energy. Experimental pulse widths were extracted from the fit of the recorded spectra, by assuming a sech shape and a transform-limited time-bandwidth product. We compared numerical and experimental data with the analytical fundamental SM soliton relationship

$$T_{0j} = \frac{\lambda|\beta_{2j}|w_j^2}{n_2 E_{sj}}, \tag{4}$$

where β_{2j} is the dispersion at j-th soliton wavelength $\lambda_j = 2\pi c/\omega_j$, with energy E_{sj}, and w_j is the effective bullet waist of the MM soliton: a best fit is obtained, when the effective waist is assumed to be equal to the input waist, i.e., by setting $w_j = w_0$. In Fig. 9, the black dashed line is obtained, in the "low-loss" regime, by inserting the soliton parameters as they are obtained from simulations. Whereas black crosses are obtained by inserting in Eq. (4) the soliton parameters given by the experiments.

In the “linear-loss” regime, for soliton energies $E_s < 15$ J, the pulse width of individual Raman MM solitons is well approximated by the SM analytical soliton formula of Eq. (4), in good agreement with numerical simulations of Section 3.2.

On the other hand, in the “nonlinear-loss” regime, that is, for $E_s > 15$ J, the black crosses in Fig. 9 show that the SM soliton formula Eq. (4) would predict a narrower pulse width, when compared to the experimentally observed soliton pulse durations. As a matter of fact, experimental spectra show that all MM Raman-shifted solitons converge to nearly same and constant (with respect to soliton energy) pulse width, with a value between 50 fs and 60 fs. At the same time, the wavelength shift of Raman solitons remains also clamped around a constant

Optics EXPRESS

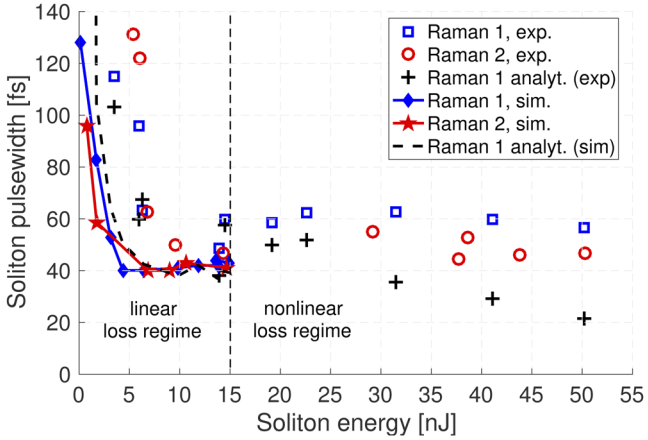

Fig. 9. Experimental data (empty squares and empty circles for solitons Raman 1 and 2, respectively) and numerical simulations (solid curves) of the output soliton FWHM pulse width vs. soliton energy; black crosses and black dashed line are obtained from Eq. (4) by using soliton parameters obtained from either experimental or simulation data, respectively.

value (see Fig. 8). The self-organization of a soliton multiplex with equal pulse widths and unequal amplitudes corresponds to a regime with minimal emission of dispersive waves (or radiation), since nonlinearity exactly balances the local dispersion (as it is determined by second and third-order dispersion) at each of the different Raman wavelengths [23].

In order to obtain a direct experimental confirmation of the time duration of MM solitons generated after fission, autocorrelation traces have been recorded. NIR and visible light was cut-off using filters. Figure 10(a) illustrates the case of two measured solitons, generated for

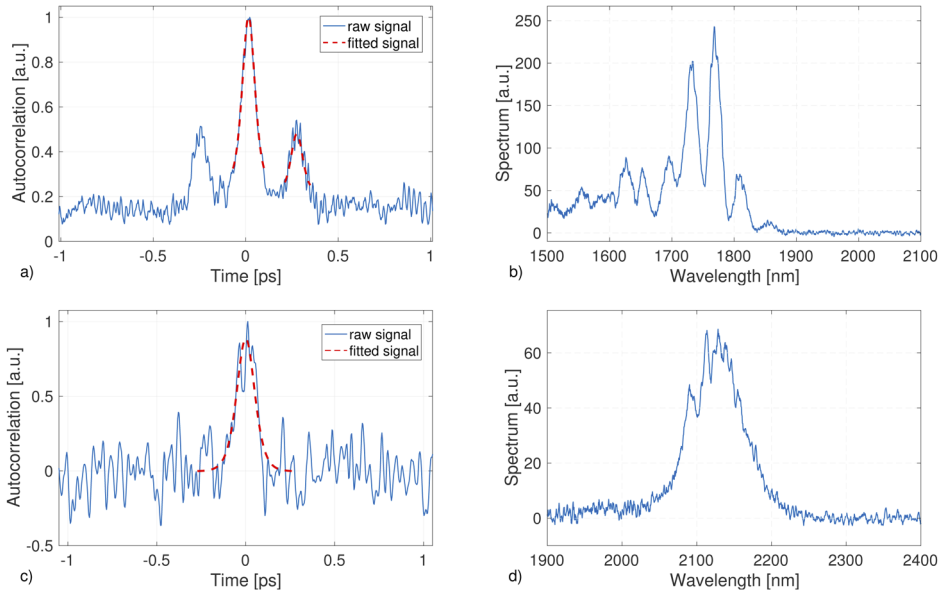

Fig. 10. Experimental autocorrelation trace a) and output spectrum b) for an input energy of 150 nJ (long-pass filtered). Autocorrelation c) and spectrum d) for an input energy of 500 nJ (band-pass filtered). Spectra are in linear scale.

Optics EXPRESS

an input pulse energy of 150 nJ. The solitons were long-pass filtered at 1500 nm in order to eliminate the super-continuum and visible fluorescence noise; the intensity autocorrelator showed pulse self-correlation and cross-correlation between two different solitons, providing a delay of 0.28 ps between pulses and an equal FWHM pulse width of 51 fs. Figure 10(b) shows the corresponding measured spectrum: the interference pattern, indicating the presence of a coherent superposition of two bound solitons (soliton molecule), is clearly visible. In other cases (not shown), spectra with non-interfering patterns have been also been observed. Figure 10(c) shows the autocorrelation of a single MM soliton, generated for 500 nJ of input energy, isolated by means of a band-pass filter centered at 2250 nm, and with 500 nm bandwidth. The Raman soliton is centered at 2110 nm, with a pulse width of 71 fs (after the filter) (see Fig. 10(d)).

3.6. Soliton transverse profile

Due to the multimode nature of the Raman solitons, it is important to analyse their transverse beam profile. The phosphors of our infrared camera (Gentec Beamage-4M-IR) are sensitive in the range of 1500-1600 nm. Therefore, we carried out the experiments of the output beam profile by using 70 femtosecond input pump pulses centered at 1450 nm with 180 kW peak power, so that a single Raman soliton could be generated exactly in the 1500-1600 nm spectral region at the output of a 30 cm long GRIN MMF. In this way, we could isolate the soliton by means of a long-pass filter at 1500 nm. This is shown in Fig. 11(e), where we can see both the full bandwidth and the soliton output spectrum. Here the gray region highlights the spectral range that is filtered out by the long-pass filter with its edge at 1500 nm.

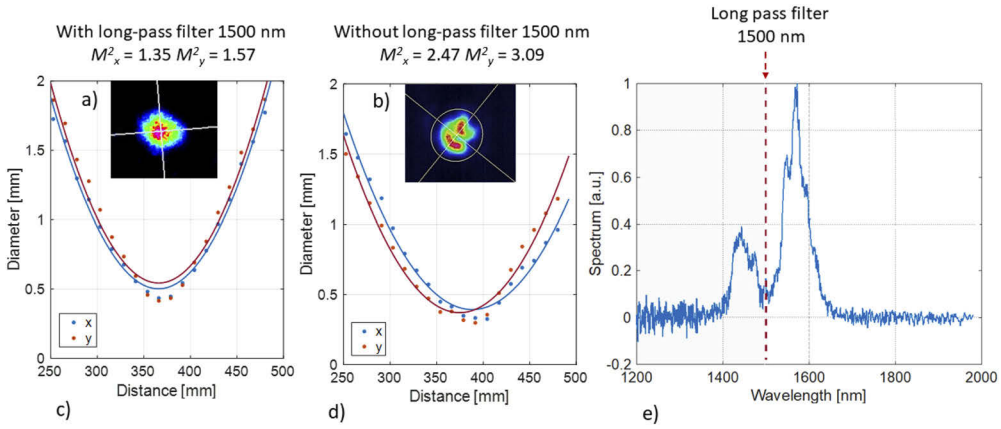

Fig. 11. Experimental analysis of the Raman soliton output transverse beam profile from 30 cm long GRIN fiber: (a) transverse profile and (c) M^2 parameter of the Raman soliton; (b,d) same as in (a,c), but for the full spectral bandwidth; (e) output spectrum , showing the region filtered out by the longpass filter at 1500 nm (grey area).

Figure 11 shows the beam profile coming out from the fiber, obtained by either isolating the soliton (see Fig. 11(a)), or across the entire spectral bandwidth (see Fig. 11(b)). For both cases, we have measured the beam quality M^2 values (see Fig. 11(c) and 11(d), respectively). As can be seen from the beam profiles and the performance of the M^2 parameter, although the profile of the filtered Raman soliton beam has a lower intensity (lower image resolution), it exhibits a much cleaner, bell-shaped spatial distribution (average M^2 = 1.46 vs. M^2 = 2.78). Remarkably, the beam quality of the output Raman soliton remains close to that of the input laser beam (M^2 = 1.3). Note that the full-bandwidth image is also affected by contributions from dispersive waves generated in the visible range (not shown in Fig. 11(e)).

Optics EXPRESS

3.7. Soliton orders

In order to match experimental and numerical data with analytical results from SM soliton theory, it was necessary in Subsection 3.5 to assume that the soliton bullet waist w_j is equal to the input beam waist w_0. This is confirmed when calculating the soliton order from the experimental and numerical data of Fig. 8 and 9. For the order of the j-th Raman MM soliton, one has

$$N_j^2 = \frac{L_{dj}}{L_{nl}} = \hat{\gamma} P_{sj} L_{dj} = \frac{\omega_j n_2 T_{0j} E_{sj}}{2\pi c |\beta_{2j}| w_j^2}, \tag{5}$$

where P_{sj} is the soliton peak power, and $E_{sj} = 2T_{0j}P_{sj}$ is the j-th soliton energy. By using either experimental or numerical parameters, we report in Fig. 12 the output soliton order as a function of its energy. Simulations in the "linear-loss" regime, in particular, converge to $N = 1$ if and only if we set $w_j = w_0$ for all wavelengths and energies. An attempt to use an effective soliton waist that is smaller than the input value (e.g., the path-average value $w_j^2 = \sqrt{C} w_0^2$), leads to orders N greater than unity, between 1 and 1.5.

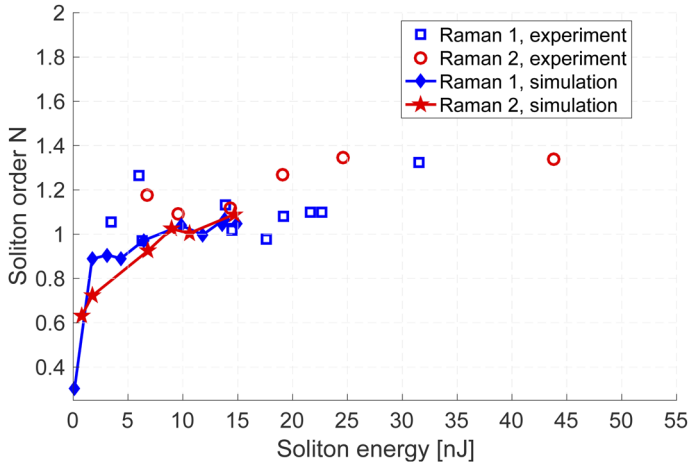

Fig. 12. Experimental (dots) and numerical (solid lines) output soliton order vs. soliton energy, assuming effective soliton waist equal to the input value w_0.

Whereas in the "nonlinear-loss" regime, for $E_{sj} > 15$ nJ, experimental soliton orders calculated with $w_j = w_0$ turn out to be in any case higher than unity, with values ranging between 1 and 1.35. This may be associated with the MM nature of the solitons, that require a higher energy with respect to SM solitons, in order to compensate for modal dispersion in addition to chromatic dispersion [12,15].

4. Conclusions

In this work, we have studied the dynamics of spatiotemporal femtosecond solitons in GRIN MM fibers at MW peak power levels approaching the critical value for beam collapse. We found that input ultra-short pulses may decay into a train of wavelength-multiplexed MM Raman solitons with different energies, but, remarkably, nearly equal temporal durations.

In the "linear-loss" regime, when generated solitons possess energies below 15 nJ, the pulse width of an individual MM Raman soliton scales with its energy according to the law for fundamental SM solitons. Moreover, the wavelength shift produced by the initial fission process largely dominates the subsequent SSFS that accompanies the propagation of Raman solitons. The experimentally observed wavelength shift of Raman solitons is in excellent agreement with both numerical simulations, and with the well-known analytical formula for the singlemode SSFS.

Optics EXPRESS

We revealed the presence of a new nonlinear propagation regime in MM fibers, which occurs for input pulse energies above 100 nJ, and up to about 550 nJ, the threshold for irreversible fiber damage. That is, for femtosecond pulses with the highest possible energies that is possible to inject in a MM GRIN fiber. In this regime, the presence of strong nonlinear multiphoton absorption by defects of the Ge-doped fiber over the first few centimeters of the fiber clamps the transmitted energy. As a result, no further spectral broadening of the generated supercontinuum, which on the long-wavelength side is determined by the SSFS of Raman solitons, occurs as the input energy grows larger than 100 nJ. In this "nonlinear-loss" regime, Raman solitons generated at different wavelengths have a common pulsewidth (50-60 fs). The Raman soliton time duration remains nearly constant, when its energy varies between 15 nJ and 50 nJ. At the same time, the soliton wavelength shift appears to be clamped to a constant value. This self-organization of the input multisoliton pulse corresponds to a natural maximum transfer of energy into its fundamental soliton components, since the generation of dispersive waves is minimized.

As a perspective for further work, the dynamics of fundamental MM Raman soliton propagation over longer fiber lengths than the case considered in our experiments (where the fiber length $L \simeq L_d$) remain to be explored. This will permit to further clarify to what extent multimodality, with the associated self-imaging and periodic compression of the beam width, permits to enhance the rate of SSFS.

Most importantly, the new propagation regime that is dominated by the presence of nonlinear loss remains to be fully characterized. Progress in our understanding of the physics of the multiphoton absorption processes, and the associated scattering of photo-luminescence, will also permit to incorporate the nonlinear loss mechanism in the propagation models.

Our findings provide a new insight in the complex dynamics of MM fiber solitons, and will be highly relevant for the development of novel fiber based sources of high-energy ultrashort pulses in the NIR and mid-infrared.

Funding

European Research Council (740355); Ministry of Science and Higher Education of the Russian Federation (14.Y26.31.0017).

Acknowledgement

The authors thank R. Crescenzi for technical support, and V. Couderc for measuring the GRIN fiber index profile. We acknowledge helpful discussions with D. Modotto, U. Minoni, V. Couderc, A. Tonello, and S. Murdoch.

Disclosures

The authors declare no conflicts of interest.

References

1. A. Hasegawa, "Self-confinement of multimode optical pulse in a glass fiber," Opt. Lett. **5**(10), 416–417 (1980).
2. B. Crosignani and P. D. Porto, "Soliton propagation in multimode optical fibers," Opt. Lett. **6**(7), 329–330 (1981).
3. B. Crosignani, A. Cutolo, and P. D. Porto, "Coupled-mode theory of nonlinear propagation in multimode and single-mode fibers: envelope solitons and self-confinement," J. Opt. Soc. Am. **72**(9), 1136–1141 (1982).
4. Y. Silberberg, "Collapse of optical pulses," Opt. Lett. **15**(22), 1282–1284 (1990).
5. K. D. Moll, A. L. Gaeta, and G. Fibich, "Self-similar optical wave collapse: Observation of the Townes profile," Phys. Rev. Lett. **90**(20), 203902 (2003).
6. S.-S. Yu, C.-H. Chien, Y. Lai, and J. Wang, "Spatio-temporal solitary pulses in graded-index materials with Kerr nonlinearity," Opt. Commun. **119**(1-2), 167–170 (1995).
7. S. Raghavan and G. P. Agrawal, "Spatiotemporal solitons in inhomogeneous nonlinear media," Opt. Commun. **180**(4-6), 377–382 (2000).

Optics EXPRESS

8. A. B. Grudinin, E. Dianov, D. Korbkin, and M. P. A D. Khaidarov, "Nonlinear mode coupling in multimode optical fibers; excitation of femtosecond-range stimulated-Raman-scattering solitons," J. Exp. Theor. Phys. Lett **47**, 356–359 (1988).
9. A. Mecozzi, C. Antonelli, and M. Shtaif, "Coupled Manakov equations in multimode fibers with strongly coupled groups of modes," Opt. Express **20**(21), 23436–23441 (2012).
10. K. Krupa, A. Tonello, A. Barthélémy, T. Mansuryan, V. Couderc, G. Millot, P. Grelu, D. Modotto, S. A. Babin, and S. Wabnitz, "Multimode nonlinear fiber optics, a spatiotemporal avenue," APL Photonics **4**(11), 110901 (2019).
11. W. H. Renninger and F. W. Wise, "Optical solitons in graded-index multimode fibres," Nat. Commun. **4**(1), 1719 (2013).
12. L. G. Wright, W. H. Renninger, D. N. Christodoulides, and F. W. Wise, "Spatiotemporal dynamics of multimode optical solitons," Opt. Express **23**(3), 3492–3506 (2015).
13. L. G. Wright, D. N. Christodoulides, and F. W. Wise, "Controllable spatiotemporal nonlinear effects in multimode fibres," Nat. Photonics **9**(5), 306–310 (2015).
14. L. G. Wright, S. Wabnitz, D. N. Christodoulides, and F. W. Wise, "Ultrabroadband dispersive radiation by spatiotemporal oscillation of multimode waves," Phys. Rev. Lett. **115**(22), 223902 (2015).
15. Z. Zhu, L. G. Wright, D. N. Christodoulides, and F. W. Wise, "Observation of multimode solitons in few-mode fiber," Opt. Lett. **41**(20), 4819–4822 (2016).
16. M. A. Eftekhar, L. G. Wright, M. S. Mills, M. Kolesik, R. A. Correa, F. W. Wise, and D. N. Christodoulides, "Versatile supercontinuum generation in parabolic multimode optical fibers," Opt. Express **25**(8), 9078–9087 (2017).
17. L. Rishøj, B. Tai, P. Kristensen, and S. Ramachandran, "Soliton self-mode conversion: revisiting Raman scattering of ultrashort pulses," Optica **6**(3), 304–308 (2019).
18. A. S. Ahsan and G. P. Agrawal, "Graded-index solitons in multimode fibers," Opt. Lett. **43**(14), 3345–3348 (2018).
19. M. Conforti, C. M. Arabi, A. Mussot, and A. Kudlinski, "Fast and accurate modeling of nonlinear pulse propagation in graded-index multimode fibers," Opt. Lett. **42**(19), 4004–4007 (2017).
20. M. Karlsson, D. Anderson, and M. Desaix, "Dynamics of self-focusing and self-phase modulation in a parabolic index optical fiber," Opt. Lett. **17**(1), 22–24 (1992).
21. A. S. Ahsan and G. P. Agrawal, "Spatio-temporal enhancement of raman-induced frequency shifts in graded-index multimode fibers," Opt. Lett. **44**(11), 2637–2640 (2019).
22. T. Hansson, A. Tonello, T. Mansuryan, F. Mangini, M. Zitelli, M. Ferraro, A. Niang, R. Crescenzi, S. Wabnitz, and V. Couderc, "Nonlinear beam self-imaging and self-focusing dynamics in a GRIN multimode optical fiber: theory and experiments," (2020). ArXiv:2005.07280.
23. Y. Kodama, A. V. Mikhailov, and S. Wabnitz, "Input pulse optimization in wavelength-division-multiplexed soliton transmissions," Opt. Commun. **143**(1-3), 53–56 (1997).
24. J. P. Gordon, "Theory of the soliton self-frequency shift," Opt. Lett. **11**(10), 662–664 (1986).
25. P. G. Kazansky, H. Inouye, T. Mitsuyu, K. Miura, J. Qiu, K. Hirao, and F. Starrost, "Anomalous anisotropic light scattering in Ge-doped silica glass," Phys. Rev. Lett. **82**(10), 2199–2202 (1999).
26. S. S. L. Pitaevskii, *Bose-Einstein Condensation* (Oxford University, 2003).
27. F. Poletti and P. Horak, "Description of ultrashort pulse propagation in multimode optical fibers," J. Opt. Soc. Am. B **25**(10), 1645–1654 (2008).
28. R. H. Stolen, J. P. Gordon, W. J. Tomlinson, and H. A. Haus, "Raman response function of silica-core fibers," J. Opt. Soc. Am. B **6**(6), 1159–1166 (1989).
29. G. P. Agrawal, *Nonlinear Fiber Optics* (Third edition, Par. 2.3, Academic Pre, 2001).
30. E. F. Shubert, *Light-Emitting Diodes* (Cambridge University, 2006).
31. L. G. Wright, Z. M. Ziegler, P. M. Lushnikov, Z. Zhu, M. A. Eftekhar, D. N. Christodoulides, and F. W. Wise, "Multimode nonlinear fiber optics: Massively parallel numerical solver, tutorial, and outlook," IEEE J. Sel. Top. Quantum Electron. **24**(3), 1–16 (2018).
32. F. M. Mitschke and L. F. Mollenauer, "Discovery of the soliton self-frequency shift," Opt. Lett. **11**(10), 659–661 (1986).